Planetary geostrophic Boussinesq dynamics: barotropic flow, baroclinic instability and forced stationary waves

Stamen I. Dolaptchiev*, Ulrich Achatz

Institut für Atmosphäre und Umwelt, Goethe-Universität Frankfurt, Frankfurt am Main, Germany

Thomas Reitz

Max-Planck-Institut für Meteorologie, Hamburg, Germany

* *Corresponding author address:* Institut für Atmosphäre und Umwelt, Fachbereich Geowissenschaften/Geographie, Goethe-Universität, Altenhöferallee 1, 60438 Frankfurt/Main, Germany

E-mail: dolaptchiev@iau.uni-frankfurt.de

Generated using v4.3.2 of the AMS LATEX template

ABSTRACT

Motions on planetary spatial scales in the atmosphere are governed by the planetary geostrophic equations. However, not much attention has been paid to the interaction between the baroclinic and barotropic flow within the planetary geostrophic scaling. This is the focus of the present study by utilizing planetary geostrophic equations for a Boussinesq fluid supplemented by a novel evolution equation for the barotropic flow. The latter is effected by meridional momentum flux due to baroclinic flow and drag by the surface wind. The barotropic wind on the other hand affects the baroclinic flow through buoyancy advection. By relaxing towards a prescribed buoyancy profile the model produces realistic major features of the zonally symmetric wind and temperature fields. We show that there is considerable cancelation between the barotropic and the baroclinic surface zonal mean zonal wind. The linear and nonlinear model response to steady diabatic zonally asymmetric forcing is investigated. The arising stationary waves are interpreted in terms of analytical solutions. We also study the problem of baroclinic instability on the sphere within the present model.

1. Introduction

Using scale considerations Burger (1958) suggested that for atmospheric motions on planetary scales, i.e., scales comparable with the radius of the Earth, the vorticity is quasi-stationary and the vorticity equation takes the form of a balance between the divergence of the horizontal wind and the advection of planetary vorticity. Later Phillips (1963) proposed for the description of planetary scale dynamics the planetary geostrophic equations (PGE), or geostrophic motions of type two. In the PGE the pressure is hydrostatically balanced and the horizontal wind is in geostrophic balance, where the full variations of the Coriolis parameter f are considered. The vertical velocity in the anelastic approximation of the PGE results solely from variations of f and there is only one prognostic equation, namely for the temperature. Because of their reduced complexity the PGE are part of the atmospheric module in some Earth system models of intermediate complexity (e.g. Petoukhov et al. 2000; Totz et al. 2018), allowing numerically efficient long-term climate simulations (for examples see Ganopolski and Rahmstorf (2001); Claussen et al. (2002); Petoukhov et al. (2005)).

Only recently, the range of validity of the PGE has been revised using currently available reanalysis data (Egger and Hoinka 2017) and simplified GCM simulations (Dolaptchiev and Klein 2013). The latter authors found from spectrally decomposed fields, that the horizontal fluxes of relative and planetary vorticity are nearly divergence free on the planetary scale. Egger and Hoinka (2017) showed that the vertical velocity from the PGE captures the stationary features in the tropospheric zonal perturbations. However, the standard deviation of the vertical velocity was considerably underestimated, due to the missing synoptic scale dynamics in the PGE. The important effect of the synoptic eddies has been incorporated in the PGE using multiple scale asymptotics (Pedlosky 1984; Dolaptchiev and Klein 2013; Boljka and Shepherd 2018) and statistical-dynamical approach (Petoukhov et al. 2003; Coumou et al. 2011; Totz et al. 2018).

Despite the popularity of the PGE not much attention has been paid to the evolution of the barotropic flow under the planetary geostrophic scaling. As stated by Bresch et al. (2006) the PGE do not represent a closed set of equations and an additional evolution equation for the barotropic pressure has been proposed there to close the system. Using asymptotic expansion Dolaptchiev and Klein (2009) have generalized the closure to the case of fully compressible flow with variable Coriolis parameter. The derived closure has the form of prognostic equation for the barotropic vorticity and is a dynamical alternative to other diagnostic closures (e.g. Petoukhov et al. 2000). This study is a first attempt to address the effect of the closure on the planetary geostrophic dynamics by utilizing numerical simulations of a Boussinesq fluid on the sphere.

In addition, in the present study the linear and nonlinear response of the PGE model to steady diabatic forcing is considered. The arising stationary waves are interpreted in terms of analytical solutions. We also study the problem of baroclinic instability within the PGE. This was first done by Wiin-Nielsen (1961), but to our knowledge the problem on the sphere has not been considered yet. The latter is in contrast to quasi-geostrophic or primitive equations dynamics, where a large body of theoretical work exists on the topic (e.g. Hollingsworth 1975; Simmons and Hoskins 1976; Baines and Frederiksen 1978).

This paper is organized as follows: In Sec. 2 an asymptotic derivation of the PGE and the equation for the barotropic dynamics is presented. The representation of diabatic and frictional effects as well as a summary of the nonlinear and linear model equations can be found in Sec. 3. The nonlinear model simulations are discussed in Sec. 4 for different model configurations. In Sec. 5 analytical wave solutions are presented and compared with the linear/nonlinear numerical simulations, also the problem of baroclinic instability is studied there. Concluding discussions can be found in Sec. 6.

2. Asymptotic derivation

Using asymptotic analysis the PGE were derived in Dolaptchiev and Klein (2009) from the full compressible fluid flow equations, here for the first time the evolution equation for the barotropic pressure is studied within the PGE. In order to simplify the analysis we consider as a starting point the hydrostatic Boussinesq equations. These equations are isomorphic to the primitive equations in pressure coordinates (Vallis 2006). Although the Boussinesq approximation is limited to vertical scales smaller than the scale height of the atmosphere, e.g. see the recent work by Egger and Hoinka (2018) on the validity of the incompressibility assumption, the Boussinesq equations are widely used for studying the large-scale circulation (e.g. Held and Hou 1980; Vallis 2006). The nondimensional governing equations for a Boussinesq fluid on the sphere are

$$\frac{\partial \vec{u}}{\partial t} + \vec{u}\cdot\nabla\vec{u} + w\frac{\partial \vec{u}}{\partial z} + \frac{1}{\varepsilon}\vec{f}\times\vec{u} = -\frac{1}{\varepsilon}\nabla\Phi + \vec{S}_u\,, \tag{1}$$

$$\frac{\partial \Phi}{\partial z} = b\,, \tag{2}$$

$$\nabla\cdot\vec{u} + \frac{\partial w}{\partial z} = 0\,, \tag{3}$$

$$\frac{\partial b}{\partial t} + \vec{u}\cdot\nabla b + w\frac{\partial b}{\partial z} = S_b\,, \tag{4}$$

where $\vec{u} = (u, v)$ denotes the horizontal velocity vector, w vertical velocity, Φ pressure fluctuations divided by reference density, b buoyancy, $\vec{f} = \vec{e}_r f$ with the Coriolis parameter f and the radial unit vector $\vec{e}_r$. The source terms due to friction and diabatic effects are denoted by $\vec{S}_u$ and S_b, respectively. The vertical coordinate is indicated by z and in the following λ is longitude and ϕ latitude. The horizontal Nabla operator is defined as $\nabla = (\frac{1}{a\cos\phi}\frac{\partial}{\partial\lambda}, \frac{1}{a}\frac{\partial}{\partial\phi})$ and for the horizontal divergence of $\vec{u}$ we have $\nabla\cdot\vec{u} = \frac{1}{a\cos\phi}(\frac{\partial u}{\partial\lambda} + \frac{\partial \cos\phi v}{\partial\phi})$, where a is the radius of the Earth. For the nondimensionalization of the variables a reference horizontal velocity of $U = 10\,\mathrm{ms}^{-1}$ and a planetary horizontal length scale of $L = 10^7$ m is used. With the above scales the Rossby number $\varepsilon = U/f_0 L$, where f_0 denotes the Coriolis parameter at 45° N, takes a value of about 10^{-2}. The reference value for the vertical velocity W is set to the standard value $W = HU/L$, where $H = 10^4$ m is the scale height of the atmosphere. The normalized pressure Φ and the buoyancy are nondimensionalized using $P = LUf_0$ and $B = P/H$, respectively, in order to assure geostrophic and hydrostatic balance to leading order. The potential temperature θ can be computed from buoyancy using $b = g(\theta - \theta_0)/\theta_0$, where g is gravity acceleration and θ_0 a constant reference potential temperature. Note that the small parameter ε and the characteristic scales used in this paper differ from the ones in Dolaptchiev and Klein (2009, 2013). In the latter studies an unified asymptotic approach is utilized, where the characteristic quantities for nondimensionalization are valid for a variety of flow regimes. To keep the present asymptotic analysis concise, here we start with characteristic scales, as described above, appropriate for planetary scale motions.

We assume that each dependent variable from (1)- (4) can be represented as an asymptotic series in terms of ε

$$\mathscr{U}(\lambda,\phi,z,t;\varepsilon) = \sum_{i=0}^{\infty} \varepsilon^i \mathscr{U}^{(i)}(\lambda,\phi,z,t)\,, \tag{5}$$

where $\mathscr{U} = (u, v, w, b, \Phi, S_b, \vec{S}_u)$. Substituting the ansatz above in (1)- (4), we obtain as leading order nontrivial asymptotic equations the planetary geostrophic equations

$$\vec{f} \times \vec{u} = -\nabla\Phi\,, \tag{6}$$

$$\frac{\partial \Phi}{\partial z} = b\,, \tag{7}$$

$$\nabla \cdot \vec{u} + \frac{\partial w}{\partial z} = 0\,, \tag{8}$$

$$\frac{\partial b}{\partial t} + \vec{u} \cdot \nabla b + w\frac{\partial b}{\partial z} = S_b\,, \tag{9}$$

where the zero superscript in all dependent variables was dropped. Next, the flow is separated into barotropic and baroclinic part. E.g. for the horizontal wind we write

$$\vec{u} = \langle\vec{u}\rangle_z + \vec{u}' , \tag{10}$$

where the baroclinic part is marked by a prime and the barotropic one is defined as

$$\langle\vec{u}\rangle_z = \frac{1}{z_a}\int\limits_0^{z_a} dz\vec{u} , \tag{11}$$

with z_a denoting the height of the atmosphere. Averaging vertically (8) and applying rigid lid boundary conditions one obtains

$$\nabla\cdot\langle\vec{u}\rangle_z = 0 . \tag{12}$$

By taking the curl of (6), one obtains vanishing divergence of the planetary vorticity flux

$$\nabla\cdot f\vec{u} = 0 , \tag{13}$$

which reads for the barotropic component

$$\nabla\cdot f\langle\vec{u}\rangle_z = 0 . \tag{14}$$

From (12) and (14) it follows that $\langle v\rangle_z$ vanishes and $\langle u\rangle_z$ does not depend on longitude

$$\langle u\rangle_z = \langle u\rangle_z(\phi,t) , \tag{15}$$

$$\langle v\rangle_z = 0 . \tag{16}$$

From (6), (8) and (10) the baroclinic wind satisfies

$$\vec{u}' = \frac{\vec{e}_r}{f}\times\nabla\Phi' , \tag{17}$$

$$w' = w = -\int\limits_0^z \nabla\cdot\vec{u}'\,dz , \tag{18}$$

where in the last equation $w = 0$ at $z = 0$ was used. For a given buoyancy field the baroclinic part of Φ can be found by integrating the hydrostatic balance (7)

$$\Phi'(\lambda,\phi,z,t) = \int_0^z b(\lambda,\phi,\eta,t)\, d\eta - \frac{1}{z_a}\int_0^{z_a} dz \int_0^z b(\lambda,\phi,\eta,t)\, d\eta\,. \tag{19}$$

Thus, (9) gives a prediction of b from which $\vec{u}'$ and w can be determined. However, in order to determine the evolution of the vertically averaged zonal wind field $\langle u \rangle_z$, we have to consider the next order asymptotic equations. From (1) and (3) we obtain for the $\mathscr{O}(1)$ zonal momentum equation and the $\mathscr{O}(\varepsilon)$ continuity equation

$$\frac{\partial u}{\partial t} + \vec{u}\cdot\nabla u + w\frac{\partial}{\partial z}u - \frac{uv}{a}\tan\phi - f v^{(1)} = -\frac{1}{a\cos\phi}\frac{\partial}{\partial\lambda}\Phi^{(1)} + S_u^{(0)}\,, \tag{20}$$

$$\nabla\cdot\vec{u}^{(1)} + \frac{\partial w^{(1)}}{\partial z} = 0\,. \tag{21}$$

Averaging (21) over λ and z and applying vanishing vertical velocity at the top and at the bottom yields

$$\left\langle v^{(1)} \right\rangle_{z,\lambda} = 0\,. \tag{22}$$

Here the vertical and zonal mean of $v^{(1)}$ is defined as

$$\left\langle v^{(1)} \right\rangle_{z,\lambda} = \frac{1}{2\pi z_a}\int_0^{z_a} dz \int_0^{2\pi} d\lambda\, v^{(1)}\,. \tag{23}$$

By applying $-\frac{1}{a\cos\phi}\frac{\partial\cos\phi}{\partial\phi}$ (20), averaging the result zonally and vertically and making use of (22), we derive a vorticity equation for the barotropic component of the flow

$$\frac{\partial}{\partial t}\langle\zeta\rangle_{z,\lambda} + \nabla\cdot\langle\vec{u}\zeta\rangle_{z,\lambda} + \vec{e}_r\cdot\nabla\times\left\langle w\frac{\partial}{\partial z}\vec{u}\right\rangle_{z,\lambda} = \langle S_\zeta\rangle_{z,\lambda}\,, \tag{24}$$

where the vorticity is defined as $\zeta = \vec{e}_r\cdot\nabla\times\vec{u}$ and the source term on the right-hand-side is given by $S_\zeta = \vec{e}_r\cdot\nabla\times\vec{S}_u^{(0)}$. Expressing all nonlinear terms on the left-hand-side of (24) in terms of meridional momentum flux yields

$$\frac{\partial}{\partial t}\langle\zeta\rangle_{z,\lambda} - \frac{1}{a\cos\phi}\frac{\partial}{\partial\phi}\frac{1}{a\cos\phi}\frac{\partial}{\partial\phi}\cos^2\phi\,\langle u'v'\rangle_{z,\lambda} = \langle S_\zeta\rangle_{\lambda,z}\,. \tag{25}$$

From the last equation one can determine the evolution of $\langle u \rangle_z$: due to (12) one can introduce a streamfunction Ψ such that

$$\langle \vec{u} \rangle_z = \vec{e}_r \times \nabla \Psi \,, \tag{26}$$

$$\langle \zeta \rangle_{z,\lambda} = \Delta \Psi = \frac{1}{a \cos\phi} \frac{\partial}{\partial \phi} \left(\frac{\cos\phi}{a} \frac{\partial \Psi}{\partial \phi} \right) . \tag{27}$$

In (27) $\Delta = \nabla^2$ denotes the horizontal Laplace operator in spherical coordinates and Ψ does not depend on λ due to (15).

Using asymptotic analysis it was shown by Boljka and Shepherd (2018) that there is a connection between the planetary scale barotropic flow equation and the preservation of angular momentum. An alternative to (25) can be derived by multiplying (20) with $a \cos\phi$ and averaging again zonally and vertically in order to obtain an equation for the vertical mean of the axial angular momentum $M = a \cos\phi u$

$$\frac{\partial}{\partial t} \langle M \rangle_{z,\lambda} + \frac{1}{a \cos\phi} \frac{\partial}{\partial \phi} \cos\phi \left\langle u' M' \right\rangle_{z,\lambda} = \langle S_m \rangle_{z,\lambda} \,, \tag{28}$$

where $S_m = a \cos\phi S_u^{(0)}$. In the last equation the angular momentum M lacks the planetary component ($\Omega a^2 \cos^2\phi$), since the zonally and vertically averaged transport of planetary angular momentum by $v^{(1)}$ from (20) vanishes anyway due to (22).

3. Model description

In this section we discuss the parameterization of diabatic and frictional effects, for that purpose the redimensionalized variables are considered.

a. Adiabatic processes

The adiabatic processes described by the term S_b in (9) are modeled with simple relaxation ansatz and diffusion

$$S_b = \frac{b_{eq} - b}{\tau} + \kappa_b \Delta b\,, \tag{29}$$

where τ is a relaxation time scale and κ_b a diffusion constant. The prescribed buoyancy profile b_{eq} is separated into zonally symmetric part and deviations from it

$$b_{eq} = \left\langle b_{eq} \right\rangle_\lambda + b_{eq}^*\,. \tag{30}$$

Here $\left\langle b_{eq} \right\rangle_\lambda$ accounts for the meridional temperature differences in a radiative equilibrium atmosphere. We utilize a relaxation profile of the form (Held and Hou 1980)

$$\left\langle b_{eq} \right\rangle_\lambda = \frac{g}{\theta_0} \left\{ -\frac{2}{3} \delta_h P_2^0(\phi) + \delta_v \left(\frac{z}{z_a} - \frac{1}{2} \right) \right\}, \tag{31}$$

where $P_n^m(\lambda, \phi)$ denotes the associated Legendre polynomial, corresponding to zonal wavenumber m and total wavenumber n. The constants $\delta_h = 100$ K and $\delta_v = 40$ K are measure for the meridional and vertical temperature gradient, respectively [1]. To the buoyancy profile $\left\langle b_{eq} \right\rangle_\lambda$ corresponds a zonal jet in thermal-wind-balance with the form

$$\left\langle u_{eq} \right\rangle_\lambda = -\frac{1}{fa} \frac{\partial}{\partial \phi} \int_0^z \left\langle b_{eq} \right\rangle_\lambda dz\,, \tag{32}$$

if zero surface wind $\left\langle u_{eq}(z=0) \right\rangle_\lambda$ is assumed.

The zonally asymmetric part b_{eq}^* from (30) models the differential heating of the atmosphere due to the land-see thermal contrast. Here we choose an idealized representation of this effect by prescribing a buoyancy anomaly which is the sum of two spherical harmonics with zonal wavenumber two

$$b_{eq}^* = \delta_p \frac{g}{\theta} \frac{2}{7} \left(P_3^2(\phi) + P_5^2(\phi) \right) \cos(2\lambda) \exp(-\alpha z)\,. \tag{33}$$

[1] Eq. (31) is similar to a Held-Suarez type relaxation profile if we set $\delta_h = 60$ K and $\delta_v = 10$ K.

The magnitude of the zonally asymmetric perturbation is set to $\delta_p = 5$ K. b^*_{eq} has its maximum at the surface at around 50° latitude and decays in the vertical with exponential decay length scale $\alpha^{-1} = 1$ km. The relaxation profile from (31), (33) is shown in Fig. 1. Note that this profile is characterized by super-rotation at the equator.

b. Frictional effects

The frictional effects on the baroclinic flow are incorporated by including turbulent eddy diffusion in the momentum equation

$$\vec{f} \times \vec{u}' = -\nabla\Phi' + \frac{\partial}{\partial z}\left(K\frac{\partial \vec{u}'}{\partial z}\right), \tag{34}$$

where K is an eddy diffusivity constant. Without frictional effects the baroclinic wind from (17) will diverge at the equator, if the gradient of Φ' does not vanish faster than the Coriolis parameter f as $\phi \to 0$. Thus, the inclusion of diffusion acts as regularization for the PGE. We have to stress, that those frictional effects are not accounted for in the present asymptotic derivation. However, when considering the equatorial region with small f, it is natural to expect that higher order effects (such as eddy dissipation) will modify the geostrophic balance. Such effects are often taken into account in studies on the tropical circulation by adding Rayleigh drag to the geostrophic balance (Matsuno 1966; Gill 1980) or diffusion (Schneider and Lindzen 1977). The value of K used in our model was set uniformly to 5 m^2s^{-1}, a value used in other idealized studies of the atmospheric circulation, e.g., Held and Hou (1980).

The baroclinic wind stress at the surface is parameterized using the drag coefficient C_D

$$K\frac{\partial \vec{u}'}{\partial z} = C_D\vec{u}' \quad \text{at } z = 0. \tag{35}$$

With the inclusion of vertical diffusion in (34) even if $\langle\Phi'\rangle_z = 0$, in general $\langle\vec{u}'\rangle_z \neq 0$. Because of this, the condition $\langle\vec{u}'\rangle_z = 0$ is imposed in the model by setting the baroclinic horizontal velocity at the upper model level z_s to

$$\vec{u}'(z_s) = -\frac{1}{\Delta z_s}\int_0^{z_t} dz \vec{u}'(z)\,. \tag{36}$$

In (36) Δz_s is the thickness of the upper layer, we refer to this layer as the stratosphere (however note that in (31) no separate assumptions on the stratification within this layer are made), and z_t marks the troposphere height. Similar boundary condition is used in other PGE based models, e.g. see Petoukhov et al. (2000) and eq. (15), (22) there. Eq. (36) is a considerable limitation of the dynamics at z_s, but as discussed in Sec. 4d this has no pronounced effect on the major features of the tropospheric dynamics.

Consistent with the eddy diffusion closure (34) and (35) , the frictional effects in the vorticity source term $\langle S_\zeta \rangle_{z,\lambda}$ from (25) are represented by Ekman friction

$$\langle S_\zeta \rangle_{z,\lambda} = -\frac{C_D}{z_a}\langle \zeta(0) \rangle_\lambda \,, \tag{37}$$

where $\zeta(0)$ denotes ζ at the lowest model level.

c. Summary of the model equations and numerical implementation

The dimensional governing equations of the planetary geostrophic model take the form of two prognostic equations for the buoyancy and barotropic vorticity

$$\frac{\partial b}{\partial t} + \vec{u}\cdot\nabla b + w\frac{\partial b}{\partial z} = \frac{b_{eq} - b}{\tau} + \kappa_b \Delta b\,, \tag{38}$$

$$\frac{\partial}{\partial t}\langle \zeta \rangle_{z,\lambda} - \frac{1}{a\cos\phi}\frac{\partial}{\partial \phi}\frac{1}{a\cos\phi}\frac{\partial}{\partial \phi}\cos^2\phi \langle u'v' \rangle_{z,\lambda} = -\frac{C_D}{z_a}\langle \zeta(0) \rangle_{z,\lambda}\,, \tag{39}$$

and diagnostic relations for Φ' and baroclinic/barotropic wind components

$$\Phi' = \int_0^z b\, d\eta - \frac{1}{z_a}\int_0^{z_a} dz \int_0^z b\, d\eta\,. \tag{40}$$

$$\vec{f}\times\vec{u}' = -\nabla\Phi' + \frac{\partial}{\partial z}\left(K\frac{\partial \vec{u}'}{\partial z}\right), \tag{41}$$

$$w = -\int_0^z \nabla\cdot\vec{u}'\, dz\,, \tag{42}$$

$$\langle u\rangle_z = -\frac{1}{a}\frac{\partial}{\partial\phi}\Delta^{-1}\langle\zeta\rangle_{z,\lambda}\,. \tag{43}$$

In (39)-(42) the primed variables indicate deviations from the vertical, as defined in (10) and (11). We use (unless otherwise stated) horizontal spectral discretization with a triangular truncation of T21 and five equidistant layers in the vertical with layer thickness of $\Delta z = 2$ km. The variables b, ζ and $\vec{u}$ are defined at the centers of the layers and w at the interfaces. Centered differences are used for the vertical discretization. As initial condition we set b to the relaxation profile $\langle b_{eq}\rangle_\lambda$ with superimposed small zonal perturbation (33) with $\delta_p = 1$ K and $\alpha = 0$. The initial barotropic wind $\langle u\rangle_z$ is determined from the vertical integral of (32). The model parameters are summarized in table 1. We integrate the model for 10^4 days, after 300 days a steady state is reached and we use for the analysis data from this state only.

d. Linear model

We linearize (38) around a zonally symmetric stationary basic state given by

$$b = \bar{b}(\phi, z)\,, \tag{44}$$

$$u = \bar{u}(\phi, z)\,, \tag{45}$$

$$v = w = 0\,, \tag{46}$$

and obtain

$$\frac{\partial b^*}{\partial t} + \frac{\bar{u}}{a\cos\phi}\frac{\partial b^*}{\partial \lambda} + \frac{v^*}{a}\frac{\partial \bar{b}}{\partial \phi} + w^*\frac{\partial \bar{b}}{\partial z} = \frac{b^*_{eq} - b^*}{\tau} + \kappa_b \Delta b^* , \tag{47}$$

where an asterisk denotes the perturbations from the basic state. In (47) we neglected the tendency of the basic state due to frictional and diabatic source terms. Note that without source terms the zonally symmetric basic state from (44)-(46) is a stationary solution of the model equations. If source terms are omitted in the linearization of the barotropic vorticity equation, the tendency of $\langle \zeta^* \rangle_{z,\lambda}$ disappears as well due to (46). In this case (47) describes the complete linear dynamics of the system. We look for normal mode solutions of the horizontally and vertically discretized version of (47). All fields are represented as a truncated series of spherical harmonics, e.g. for b^* at vertical level z_l this series reads

$$b^*(\lambda, \phi, z_l, t) = \sum_{k=-T}^{T} \sum_{n=|k|}^{T} b_n^k(z_l) P_n^k(\phi) \exp\{i(k\lambda - \omega t)\} ,$$

with T denoting the spectral truncation, ω frequency and $b_n^k(z_l)$ the spectral coefficients. Thus, (47) is written as system of linear equations

$$-i\omega\vec{b} = L\vec{b} + \frac{\vec{b}_{eq}}{\tau} , \tag{48}$$

where the vector $\vec{b}$ has as entries the coefficients $b_n^k(z_l)$, L is a matrix dependent on the basic state and $\vec{b}_{eq}$ describes the inhomogeneity of the equation. We refer to (48) as the linear model associated with the PGE model from Sec. 3c.

4. Numerical simulations

a. Standard setup

In the following, we refer to the setup of the source terms, described in the previous section, as standard setup. The resulting stationary zonally averaged circulation in the model shows realistic key features of the temperature and wind fields as displayed in Fig. 2a. The westerly jets are in thermal wind balance and have a jet maximum of 40 ms^{-1} at around 30°, at the model top. At the surface weak easterlies in the tropics and westerlies in mid-latitudes are visible. The baroclinic wind u' (not shown) is easterly in the lower atmosphere, westerly in the upper atmosphere and has a linear vertical shear. In order to study the meridional overturning circulation we introduce a stream function ψ satisfying $\langle v \rangle_\lambda = -\frac{1}{\cos\phi}\frac{\partial \psi}{\partial z}, \langle w \rangle_\lambda = \frac{1}{a\cos\phi}\frac{\partial \psi}{\partial \phi}$. The Hadley cell depicted in Fig. 2b is too broad and extends into high-latitudes. Note, that due to (41) the meridional circulation is explained entirely in terms of viscous axisymmetric models (e.g. Schneider and Lindzen 1977) and misses the important effect by the advection of relative angular momentum (see Held and Hou (1980) for a discussion).

The stationary zonal anomaly of the temperature field in the lower and upper atmosphere is displayed in Fig. 3. Each individual extremum can be associated with an extremum in the forcing and there is no generation of wave trains as in the quasi-geostrophic dynamics. There is nearly no vertical tilt of the disturbances but there is a phase shift of about 30° to the east with respect to the forcing. The stationary wave amplitude is small and decays rapidly with height. The wave amplitude is considerably underestimated when comparing with quasi-stationary waves in the atmosphere. This discrepancy might result from the Boussinesq approximation and from the vertical profile of the forcing considered here.

The time averaged meridional momentum transport is analyzed in Fig. 4a. For that purpose the zonally and vertically averaged momentum flux $\langle u'v' \rangle_{z,\lambda}$, entering the barotropic equation (39), is separated into a contribution from the zonally symmetric circulation (mean meridional overturning circulation) and from zonally asymmetric part, defined as eddies. Fig. 4a shows that the meridional momentum transport by the eddies is not significant. Whereas the magnitude of the momentum flux by the zonally symmetric circulation is realistic, the one by the eddies is considerably underestimated when comparing with observations (Peixoto and Oort 1992).

Next, we consider the budget in the barotropic momentum equation, which determines the zonally averaged surface zonal wind. By dividing (28) by $a\cos\phi$ and substituting the source term S_m corresponding to (37), one obtains the following barotropic momentum equation for stationary motion

$$\frac{1}{a\cos^2\phi}\frac{\partial}{\partial\phi}\cos^2\phi\left\langle u'v'\right\rangle_{z,\lambda} = -\frac{C_D}{z_a}\left(\langle u\rangle_z + \left\langle u'(0)\right\rangle_\lambda\right) . \tag{49}$$

The term on the left-hand-side describes the contribution from the momentum flux divergence and from the metric term (4.th term on the left-hand-side of (20)), whereas the two terms on the right-hand-side account for Ekman friction by the barotropic and baroclinic flow. The contributions of the different terms are displayed in Fig. 4b. The barotropic wind and the baroclinic surface wind have opposite signs everywhere outside the tropics and there is considerable cancellation between the two components. The Ekman friction by the full surface zonal wind $\langle u(0)\rangle_\lambda = \langle u\rangle_z + \langle u'(0)\rangle_\lambda$ balances the momentum flux term on the right-hand-side of (49) (except at the poles due to interpolation errors).

The PGE generate transient disturbances by baroclinic instability (see Sec. 5e), which propagate with the mean flow and are concentrated in the subtropical and tropical region. Those transients are damped in the standard model configuration by choosing sufficiently high diffusivity κ_b[2]. We also performed simulations allowing for baroclinic eddies with zonal wavenumber 10 and obtained qualitatively similar results (not shown) as described in this section.

[2]The value of κ_b considered here, see tab. 1, corresponds to a damping time scale of $3/4$ day of the spherical harmonics with the highest total wavenumber.

b. The effect of the barotropic closure

In order to assess the effect of the evolution equation for the barotropic flow on the circulation, we perform simulation where the closure (39) is omitted. Without closure $\langle u \rangle_z$ does not change from its initial value and the total zonal mean zonal wind in the model is too strong and shows super-rotation at the equator, see Fig. 5. Whereas the zonally symmetric baroclinic flow remains unchanged, the amplitude of the stationary zonal perturbations is reduced by a factor of 50 %, if the temperature fields are considered (not shown). The latter are affected by the barotropic wind through buoyancy advection.

c. Sensitivity with respect to the diffusion coefficient K

Since in the free atmosphere the effect due to eddy dissipation should be negligible, we perform simulation with nonuniform diffusion coefficient K in (41). In particular, we choose for the meridional dependence of K a Gaussian-profile centered at the equator

$$K(\phi) = K_0 e^{-\frac{\phi^2}{2\sigma_K^2}} \tag{50}$$

with $K_0 = 5m^2s^{-1}$, corresponding to the uniform K value in the standard setup. By setting $\sigma_K = 4^\circ$, K decreases rapidly away from the equator. Note, that the equatorial region should have non-vanishing K to prevent the singularity of the PGE discussed earlier. Nearly no difference is visible in the zonally averaged temperature and wind fields from Fig. 6a compared to the standard setup (Fig. 2a). There is some weakening of the Hadley cell observed, see Fig. 6b and 2b .

We have also performed simulations with uniform K, but taking $\frac{1}{10}$th of the reference magnitude $5m^2s^{-1}$. The resulting circulation (not shown) was nearly unaltered compared to the standard setup and we conclude that the results are not sensitive with respect to the diffusion coefficient

K. Simulations were also carried out by replacing the diffusion in (41) by Rayleigh friction and qualitatively similar results (not shown) were obtained.

d. Sensitivity with respect to resolution

The effect of the upper boundary condition (36) on the dynamics is studied by performing a model simulation with doubled number of vertical levels (10 levels with $\Delta z = 1$ km), where the stratosphere is resolved by two layers instead of a single layer in the standard setup. In the stratosphere the vertical structure of the baroclinic winds $\vec{u}'$ is set to a linear profile. The latter is determined by imposing $\langle \vec{u}' \rangle_z = 0$ and requiring continuity of $\vec{u}'$ at the tropopause. In the special case of single stratospheric layer this approach reduces to the one described by (36). The convergence of the results with respect to horizontal resolution was verified by considering T42 spectral resolution. The zonally averaged circulation in the model is summarized in Fig. 7. All main features in the circulation remain the same as in the standard setup. The maximum of the stream function ψ_{max} from the meridional overturning circulation (Fig. 7b) is slightly reduced from $2172.2\,m^2/s$ (standard setup) to $1999.8\,m^2/s$. No changes in the zonally asymmetric disturbances are observed (not shown).

In addition, model run with an extended height of the troposphere to $z_t = 10$ km ($z_a = 12$ km) was performed, where the number of vertical levels was increased to 12 ($\Delta z = 1$ km). In the simulation the westerly jets increase further above 10 km and reach maximum of about 52 m/s (not shown). There is an intensification of the Hadley cell ($\psi_{max} = 2306.8\ m^2/s$), where the upper branch shifts to higher altitudes (not shown).

5. Linear analysis

Many aspects of the forced stationary waves in the atmosphere can be explained using linear theory within the quasi-geostrophic framework (e.g. Held 1983; Pedlosky 1987). For the PGE topographically and thermally forced stationary wave solutions were recently presented by Egger and Hoinka (2017). Here wave solutions of the linear PGE Boussinesq model are used to interpret the results from the numerical simulations in Section 4.

In the following we consider the linearized equations with $\kappa_b = K = C_D = 0$ and a basic state from (44)-(46) with $\bar{u} = \bar{u}(\phi)$, $\frac{\partial \bar{b}}{\partial z} = const$ and $\frac{\partial \bar{b}}{\partial \phi} = 0$. Differentiating (47) with respect to z, using the thermal wind relation and hydrostatic balance, yields

$$\frac{\partial}{\partial t}\frac{\partial^2}{\partial z^2}\Phi^* + \frac{\bar{u}}{a\cos\phi}\frac{\partial}{\partial \lambda}\frac{\partial^2}{\partial z^2}\Phi^* + \frac{\beta}{a\cos\phi f^2}\frac{\partial \bar{b}}{\partial z}\frac{\partial}{\partial \lambda}\Phi^* = \frac{\partial}{\partial z}S_b^*, \tag{51}$$

where Φ^* denotes the perturbation of Φ' from $\bar{\Phi}'$ and $S_b^* = (b_{eq}^* - b^*)/\tau$.

a. Free waves

Looking for solutions of the form $\Phi^* = \hat{\Phi}(\phi)\exp\{i(k\lambda + mz - \omega t)\}$ (k zonal-, m meridional wavenumber and ω frequency) and setting $S_b^* = 0$, one obtains the dispersion relation

$$\omega = \frac{1}{a\cos\phi}\left(\bar{u}k - \frac{\beta k}{m^2 f^2}\frac{\partial \bar{b}}{\partial z}\right). \tag{52}$$

This corresponds to the long-wavelength limit of Rossby waves from the quasi-geostrophic theory. The waves become stationary if $\bar{u} = \frac{\beta}{m^2 f^2}\frac{\partial \bar{b}}{\partial z}$. Note, that the left-hand-side of (51) does not involve any meridional derivatives of Φ^* and the equation decouples in meridional direction. As a consequence the waves can have arbitrary meridional structure.

b. Forced stationary waves: general case

We consider forcing of the form

$$S_b^* = \frac{b_{eq}^* - \frac{\partial}{\partial z}\Phi^*}{\tau}\,, \tag{53}$$

with $b_{eq}^* = B(\phi)\cos(k_0\lambda)e^{-\alpha z}$, which has the form of the zonally asymmetric forcing (33). The stationary form of eq. (51) divided by $\bar{u}/a\cos\phi$ is

$$\frac{\partial}{\partial\lambda}\frac{\partial^2}{\partial z^2}\Phi^* + n\frac{\partial}{\partial\lambda}\Phi^* + \hat{\gamma}\frac{\partial^2}{\partial z^2}\Phi^* = Q(\phi)\cos(k_0\lambda)e^{-\alpha z}\,, \tag{54}$$

where the following definitions were introduced

$$n = \frac{\beta}{\bar{u}f^2}\frac{\partial\bar{b}}{\partial z}\,, \tag{55}$$

$$\hat{\gamma} = \frac{a\cos\phi}{\bar{u}\tau}\,, \tag{56}$$

$$Q(\phi) = -\frac{\alpha a\cos\phi B(\phi)}{\tau\bar{u}}\,. \tag{57}$$

The rigid lid boundary conditions for Φ^* are given by the linearized version of (47) under the assumption of $\frac{\partial\bar{u}}{\partial z} = 0$ and $\kappa_b = 0$

$$\frac{\bar{u}}{a\cos\phi}\frac{\partial}{\partial\lambda}\frac{\partial}{\partial z}\Phi^* = S_b^* \quad \text{at } z = 0, z_a\,. \tag{58}$$

A particular solution of the inhomogeneous equation (54) reads

$$\Phi_p^* = Qe^{-\alpha z}\Big(A_r\cos(k_0\lambda) - A_i\sin(k_0\lambda)\Big) \tag{59}$$

where

$$A_r = \frac{\gamma\alpha^2}{k_0((\alpha^2+n)^2+\gamma^2\alpha^4)}\,, \quad A_i = \frac{-\alpha^2+n}{k_0((\alpha^2+n)^2+\gamma^2\alpha^4)} \tag{60}$$

$$\gamma = \frac{\hat{\gamma}}{k_0}\,. \tag{61}$$

The homogeneous solution to (54) takes the form

$$\Phi_h^* = e^{\mu_r z}\Big(a_1\cos(k\lambda+\mu_i z)+a_2\sin(k\lambda+\mu_i z)\Big)+e^{-\mu_r z}\Big(a_3\cos(k\lambda-\mu_i z)+a_4\sin(k\lambda-\mu_i z)\Big), \tag{62}$$

where the real numbers μ_r, μ_i satisfy $\mu = \mu_r + i\mu_i$ with $\mu^2 = -\frac{n}{1+\gamma^2}(1+i\gamma)$.

The particular solution (59) alone does not fulfill the boundary conditions (58), but together with the homogeneous solution they can be satisfied by setting $k = k_0$ in (62) and choosing appropriate constants a_j. However, the explicit form of the constants becomes soon tedious and we introduce in the following section an approximation in order to simplify the analytical expressions.

c. Forced stationary waves: no-relaxation-case

Neglecting the damping term in the buoyancy forcing, we consider here

$$S_b^* = \frac{b_{eq}^*}{\tau}. \tag{63}$$

In this case we can set in (54) $\hat{\gamma}$ to zero and the particular solution has the form

$$\Phi_p^* = \frac{Q}{k_0(\alpha^2+n)} e^{-\alpha z}\sin(k_0\lambda). \tag{64}$$

Again we have to add the corresponding homogeneous solution in order to satisfy the boundary conditions. The full solution takes the form

$$\Phi^* = \begin{cases} b_1 e^{mz}\sin(k_0\lambda) + b_2 e^{-mz}\sin(k_0\lambda) + \Phi_p^*, & \text{for } n = -m^2 < 0, \\ c_1\sin(mz)\sin(k_0\lambda) + c_2\cos(mz)\sin(k_0\lambda) + \Phi_p^*, & \text{for } n = m^2 > 0, \end{cases} \tag{65}$$

where

$$b_1 = \Gamma \frac{e^{-\alpha z_a} - e^{-m z_a}}{e^{m z_a} - e^{-m z_a}}, \tag{66}$$

$$b_2 = \Gamma \frac{e^{-\alpha z_a} - e^{m z_a}}{e^{m z_a} - e^{-m z_a}}, \tag{67}$$

$$c_1 = -\Gamma, \tag{68}$$

$$c_2 = \Gamma \frac{e^{-\alpha z_a} - \cos(m z_a)}{\sin(m z_a)}, \tag{69}$$

$$\Gamma = \frac{m Q(\phi)}{k_0 \alpha (\alpha^2 + n)}. \tag{70}$$

d. Forced stationary waves: comparison with the nonlinear model

We compare the solutions of the linearized equations, described in this Sections 5b&c, with the full nonlinear stationary model response form Sec. 4a. We consider altogether three models describing linear dynamics. The first model is the analytical solution (65) evaluated by setting the basic state zonal wind $\bar{u}(\phi)$ to the time averaged zonal mean zonal wind at 3 km height from the nonlinear simulation and setting the buoyancy vertical gradient $\frac{\partial \bar{b}}{\partial z}$ to $\frac{\partial \langle b_{eq} \rangle_\lambda}{\partial z} = \delta_v / z_a$. The second model is described by (54), but instead of solving (54) for Φ^*, we solve the equivalent equation for b^*. This has the form of (48) with $\omega = 0$, where the basic state entering L is the same as for the analytical solution (65) and $\kappa_b = K = C_D = 0$. We refer to the resulting model as the linear inviscid model. Note, that there is no vertical shear in the basic state zonal wind in this model. The third model is the stationary solution of the linear model (48) but with vertically varying basic state, where $(\bar{b}, \langle \bar{u} \rangle_z)$ are set to the time averaged profiles $(\langle b \rangle_\lambda, \langle u \rangle_z)$ from the nonlinear simulation. In addition, effects due to friction and diffusion are taken into account in the linear model by using the values of κ_b, K and C_D from the standard setup. Due to numerical reasons the solution of the linear inviscid model is computed with T42 spectral resolution, whereas for the full linear model T21 resolution is sufficient.

The results for the different models are summarized in Fig. 8 and 9. The linear model (Fig. 8d, 9d) reproduces the meridional and vertical structure of the stationary waves in the nonlinear simulation (Fig. 8a, 9a) . Small deviations in the meridional structure are visible only equatorward of 30°. The analytical solution (65) captures the large-scale structure of the stationary waves poleward of 30° but produces spurious oscillations in the tropics (Fig. 8b). Similar oscillations are observed in the inviscid linear model due to the neglected frictional effects (Fig. 8c).

Fig. 10 shows the stationary linear solutions, when the relaxation time scale τ is reduced from the standard value of 15 to 5 days. For $\tau = 5$ days the full linear model reproduces again accurately the nonlinear response (not shown). The magnitude of the analytical solution increases for smaller τ in accordance with the nonlinear solution. Further inspection showed that there is a slight increase by about 5° in the phase lag of the analytical solution with respect to the nonlinear solution. The inviscid linear model captures the nonlinear response to diabatic forcing for $\tau = 5$ days. The exact match of magnitudes at 50°, is to some extent by chance (but not the phase match). The reason is, that the basic state wind in the inviscid linear model was set to the stationary wind field at 3 km height from the nonlinear simulation, which is an arbitrary level choice. From Fig. 10 we conclude that for smaller τ the difference between the linear inviscid model and the analytical solution increases. At the same time the effect of the vertical shear (present in the linear model and not included in the linear inviscid model) becomes less important over the relaxation effect (included in both linear models).

e. Baroclinic instability within the PGE on the sphere

Up till now we considered disturbances generated by adiabatic heating, but even in the absence of forcing the PGE can produce exponentially growing disturbances by the mechanism of baroclinic instability. To study the latter process we utilize the linear model from (48) without forcing and dissipation, i.e., κ_b, K, C_D and $1/\tau$ are set to zero. As a basic state we set $(\bar{b}, \langle\bar{u}\rangle_z)$ to the time averaged profiles $(\langle b\rangle_\lambda, \langle u\rangle_z)$ from the nonlinear simulation. The results reported here are computed using T85 spectral resolution for convergence reasons.

Growth rates of the most unstable modes are shown in Fig. 11a. The growth rates increase linearly with zonal wavenumber without any bound. This is consistent with previous β-plane analysis of the PGE (Wiin-Nielsen 1961; Colin de Verdiere 1986). Since the PGE are valid on the very large spatial scales, only the results for the lowest wavenumbers should be relevant for the atmosphere. E.g. for wavenumber 3 the growth rate corresponds to e-folding time scale of about one week, which is comparable with the time scale of radiative processes. As shown in Fig. 11b the phase speed of the unstable modes nearly does not depend on the wavenumber and takes values between 1 and 4 ms^{-1}. Due to the meridional decoupling of the inviscid eigenvalue problem, as discussed below (52), the horizontal structure of the unstable modes cannot be determined. The disturbances show a westward vertical tilt of about quarter of a wavelength in the lowest atmosphere, see Fig. 12.

6. Conclusions

We present numerical simulations of the PGE for Boussinesq fluid on the sphere supplemented by a novel evolution equation for the barotropic flow. The latter is effected by meridional momentum flux due to baroclinic flow and drag by the surface wind, see (39). The barotropic wind on the other hand affects through buoyancy advection the baroclinic flow. In order to remove the singularity of the PGE at the equator, the geostrophic balance is modified by including turbulent eddy diffusion. This is a different approach compared to other PGE type models, where f is fixed at a constant value $f(\pm 15^\circ)$ in the tropical region of each hemisphere (Petoukhov et al. 2000). The model is forced by relaxation towards a prescribed buoyancy profile.

The model climatology shows westerly jets and surface tropical easterlies consistent with other Boussinesq simulations (e.g. Held and Hou 1980). Due to the inclusion of turbulent eddy momentum diffusion, the model produces a viscous Hadley cell. This overturning circulation is responsible for the meridional momentum transport, whereas the flux due to eddies is negligible. The stationary zonally averaged surface zonal wind is determined entirely by the baroclinic meridional momentum flux $\langle u'v'\rangle_{z,\lambda}$ (see (49)). There is considerable cancellation between the barotropic wind and the baroclinic surface zonal wind when time and zonal averages are considered (see Fig. 4b). It is observed that the barotropic wind affects only the zonally asymmetric part of the baroclinic flow (see Sec. 4b).

We study the response of the model to an idealized land-sea thermal forcing with exponential vertical decay. The stationary waves observed in the simulation are confined to the lower atmosphere and have no vertical tilt. It is shown that the response can be understood entirely in terms of linear dynamics. Forced stationary wave solutions within the PGE were derived by Egger and Hoinka (2017). Here we consider analytical solutions but for different forcing profile and under the Boussinesq assumption. It is shown that those solutions reproduce key features of the vertical and horizontal structure of the model response in mid-latitudes.

The analysis of Wiin-Nielsen (1961) on baroclinic instability within the PGE on a β-plane is extended to the sphere by considering growth rate, phase speed and the vertical structure of the most unstable modes. The growth rates increase linearly with wavenumber. This unbounded increase is due to the neglected relative vorticity advection in the PGE (Wiin-Nielsen 1961; Colin de Verdiere 1986) and makes the numerical treatment of the equations challenging, since the highest resolved scales are most unstable. In our model the inclusion of buoyancy diffusion introduces a cut-off in the growth rates. In the standard model configuration the baroclinic eddies are suppressed using sufficiently high diffusion. But simulations with baroclinic eddies indicate qualitatively similar results for the zonally averaged circulation.

Due to the Boussinesq assumption the wave disturbances (forced and baroclinic) in our model do not show an increase of amplitude with height as typically observed in the atmosphere. Consequently, momentum and temperature transport by the waves is underestimated. In future we plan to relax the Boussinesq approximation to account for the missing effect. This requires further analysis to pose an appropriate upper boundary condition for the model.

Another important ingredient absent in the present model is the mid-latitude synoptic-scale dynamics. In the case of small-amplitude eddies Boljka and Shepherd (2018); Boljka et al. (2018) provide a framework for studying interactions of the mean flow with planetary and synoptic scales. In the case of large-amplitude eddies, the two-scale model of Dolaptchiev and Klein (2013) would be the asymptotic consistent extension of the present planetary scale model to the synoptic scale. Interestingly, the planetary barotropic flow equation provides there the only feedback mechanism from the synoptic scale to the planetary scale. This stresses the importance for the dynamics of the barotropic closure equation considered here.

Acknowledgments. The authors thank the two reviewers for their comments and suggestions which helped to improve the manuscript. The authors are also thankful to Rupert Klein, Theodore Shepherd and Alexey Eliseev for valuable discussions and comments. SD thanks the German Research Foundation (DFG) for partial support through grant DO 1819/1-1. UA thanks DFG for partial support through grant AC 71/7-1.

References

Baines, P. G., and J. S. Frederiksen, 1978: Baroclinic instability on a sphere in two-layer models. *Quarterly Journal of the Royal Meteorological Society*, **104 (439)**, 45–68, doi:10.1002/qj.

49710443905.

Boljka, L., and T. G. Shepherd, 2018: A Multiscale Asymptotic Theory of Extratropical Wave–Mean Flow Interaction. *Journal of the Atmospheric Sciences*, **75 (6)**, 1833–1852, doi: 10.1175/JAS-D-17-0307.1.

Boljka, L., T. G. Shepherd, and M. Blackburn, 2018: On the Coupling between Barotropic and Baroclinic Modes of Extratropical Atmospheric Variability. *Journal of the Atmospheric Sciences*, **75 (6)**, 1853–1871, doi:10.1175/JAS-D-17-0370.1.

Bresch, D., D. Gérard-Varet, and E. Grenier, 2006: Derivation of the Planetary Geostrophic Equations. *Archive for Rational Mechanics and Analysis*, **182 (3)**, 387–413, doi:10.1007/s00205-006-0008-6.

Burger, A. P., 1958: Scale Consideration for Planetary Motion in the Atmosphere. *Tellus*, **10**, 195–205.

Claussen, M., and Coauthors, 2002: Earth system models of intermediate complexity: Closing the gap in the spectrum of climate system models. *Climate Dynamics*, **18**, 579–586, doi:10.1007/s00382-001-0200-1.

Colin de Verdiere, A., 1986: On mean flow instabilities within the planetary geostrophic equations. *Jour. Phys. Ocean.*, **16**, 1981–1984.

Coumou, D., V. Petoukhov, and A. V. Eliseev, 2011: Three-dimensional parameterizations of the synoptic scale kinetic energy and momentum flux in the Earth's atmosphere. *Nonlinear Processes in Geophysics*, **18 (6)**, 807–827, doi:10.5194/npg-18-807-2011.

Dolaptchiev, S. I., and R. Klein, 2009: Planetary geostrophic equations for the atmosphere with evolution of the barotropic flow. *Dynamics of Atmospheres and Oceans*, **46**, 46–61.

Dolaptchiev, S. I., and R. Klein, 2013: A multi-scale model for the planetary and synoptic motions in the atmosphere. *J. Atmos. Sci.*, **70**, 2963–2981.

Egger, J., and K.-P. Hoinka, 2017: The vertical component of the geostrophic wind. *Quarterly Journal of the Royal Meteorological Society*, **143 (704)**, 1704–1713, doi:10.1002/qj.3044.

Egger, J., and K.-P. Hoinka, 2018: Hydrostatic vertical velocity and incompressibility in the Northern Hemisphere. *Quarterly Journal of the Royal Meteorological Society*, **0 (ja)**, doi: 10.1002/qj.3452.

Ganopolski, A., and S. Rahmstorf, 2001: Rapid changes of glacial climate simulated in a coupled climate model. *Nature*, **409 (6817)**, 153–158, doi:10.1038/35051500.

Gill, A. E., 1980: Some simple solutions for heat-induced tropical circulation. *Quarterly Journal of the Royal Meteorological Society*, **106 (449)**, 447–462, doi:10.1002/qj.49710644905.

Held, I. M., 1983: Stationary and quasi-stationary eddies in the extratropical troposphere: Theory. *Large-scale dynamical processes in the atmosphere*, 127–168.

Held, M., and A. Hou, 1980: Nonlinear axially symmetric circulation in a nearly inviscid limit. *J. Atmos. Sci.*, **37**, 515–548.

Hollingsworth, A., 1975: Baroclinic instability of a simple flow on the sphere. *Quarterly Journal of the Royal Meteorological Society*, **101 (429)**, 495–528, doi:10.1002/qj.49710142908.

Matsuno, T., 1966: Quasi-Geostrophic Motions in the Equatorial Area. *Journal of the Meteorological Society of Japan. Ser. II*, **44 (1)**, 25–43, doi:10.2151/jmsj1965.44.1_25.

Pedlosky, J., 1984: The Equations for Geostrophic Motion in the Ocean. *Jour. Phys. Ocean.*, **14**, 448–455.

Pedlosky, J., 1987: *Geophysical Fluid Dynamics*. 2nd ed., Springer Verlag, New York.

Peixoto, J., and A. Oort, 1992: *Physics of Climate*. Springer Verlag, New York.

Petoukhov, V., A. Ganopolski, V. Brovkin, M. Claussen, A. Eliseev, C. Kubatzki, and S. Rahmstorf, 2000: CLIMBER-2: A Climate System Model of Intermediate Complexity. Part I: Model Description and Performance for Present Climate. *Climate Dynamics*, **16**, 1–17.

Petoukhov, V., A. Ganopolski, and M. Claussen, 2003: *POTSDAM - a Set of Atmosphere Statistical- Dynamical Models: Theoretical Background*. Potsdam Institute of Climate Impact Research, Report 81, http://www.pik-potsdam.de/research/publications/pikreports.

Petoukhov, V., and Coauthors, 2005: EMIC Intercomparison Project (EMIP CO_2): Comparative analysis of EMIC simulations of climate, and of equilibrium and transient responses to atmospheric CO_2 doubling. *Climate Dynamics*, **25**, 363–385, doi:10.1007/s00382-005-0042-3.

Phillips, N. A., 1963: Geostrophic Motion. *Reviews of Geophysics*, **1**, 123–175.

Schneider, E., and R. Lindzen, 1977: Axially symmetric steady-state models of the basic state for instability and climate studies. Part I linearized calculations. *J. Atmos. Sci.*, **34**, 263–279.

Simmons, A. J., and B. J. Hoskins, 1976: Baroclinic Instability on the Sphere: Normal Modes of the Primitive and Quasi-Geostrophic Equations. *Journal of the Atmospheric Sciences*, **33 (8)**, 1454–1477, doi:10.1175/1520-0469(1976)033⟨1454:BIOTSN⟩2.0.CO;2.

Totz, S., A. V. Eliseev, S. Petri, M. Flechsig, L. Caesar, V. Petoukhov, and D. Coumou, 2018: The dynamical core of the Aeolus 1.0 statistical–dynamical atmosphere model: Validation and parameter optimization. *Geoscientific Model Development*, **11 (2)**, 665–679, doi:https://doi.org/10.5194/gmd-11-665-2018.

Vallis, G. K., 2006: *Atmospheric and Oceanic Fluid Dynamics*. Cambridge University Press, Cambridge, U.K.

Wiin-Nielsen, A., 1961: A preliminary study of the dynamics of transient, planetary waves in the atmosphere. *Tellus*, **13**, 320–333.

LIST OF TABLES

TABLE 1. Model parameters from the standard setup

δ_h	100 K
δ_v	40 K
δ_p	5 K
α	1 km^{-1}
z_a	10 km
z_s	9 km
Δz_s	2 km
τ	15 days
κ_b	1.356 10^6 m^2 s^{-1}
C_D	0.005 m s^{-1}
K	5 m^2/s
g	9.81 m s^{-2}
a	6371 km
θ_0	288.15 K

LIST OF FIGURES

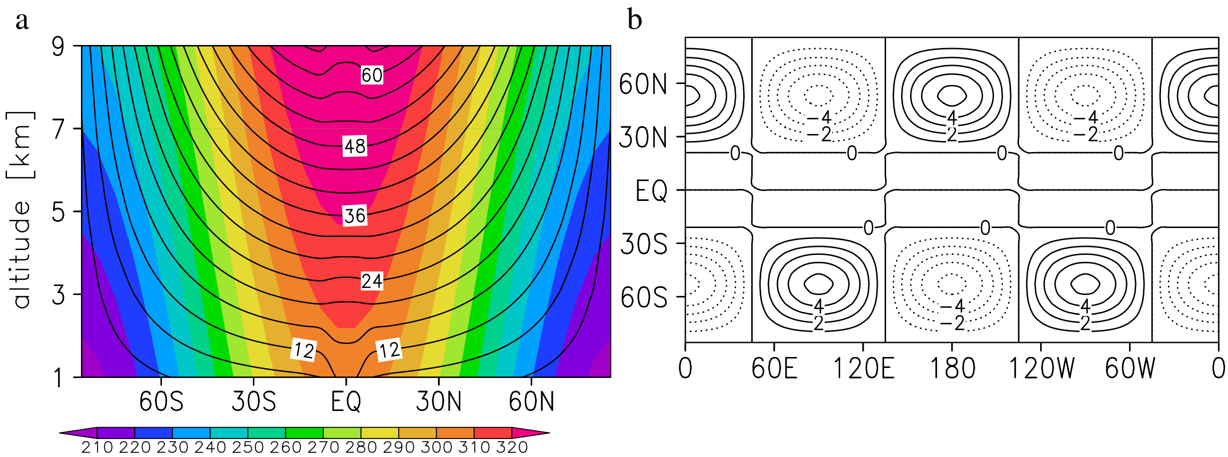

FIG. 1. (a) Zonally symmetric potential temperature (shading) and zonal wind (contours) corresponding to the relaxation profile from (31). (b) Zonally asymmetric potential temperature distribution at 1 km height corresponding to the relaxation profile from (33).

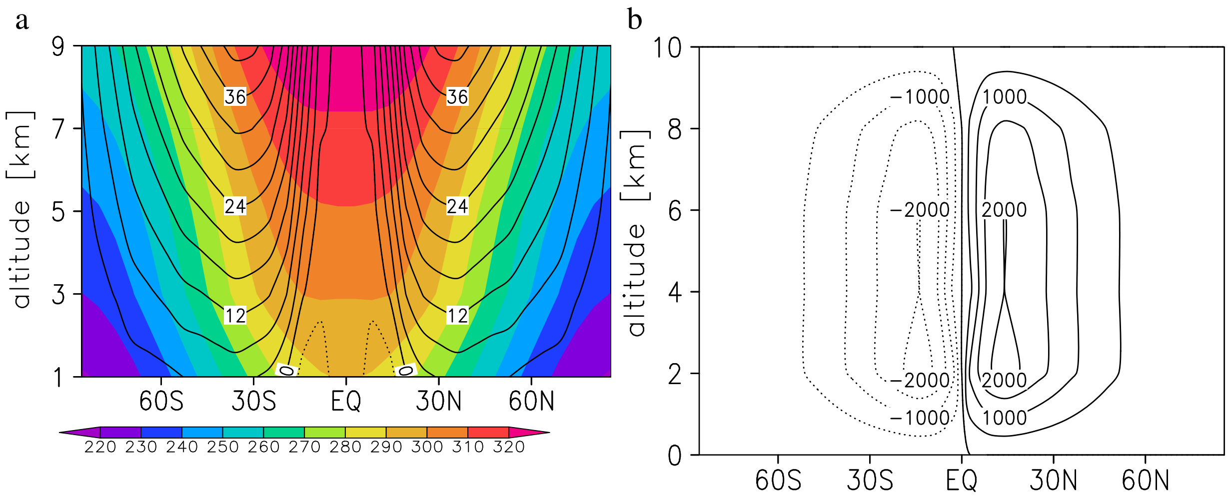

FIG. 2. Time mean zonal mean circulation in the PGE model: (a) zonal wind (contours) and potential temperature (shading); (b) stream function of the meridional overturning circulation.

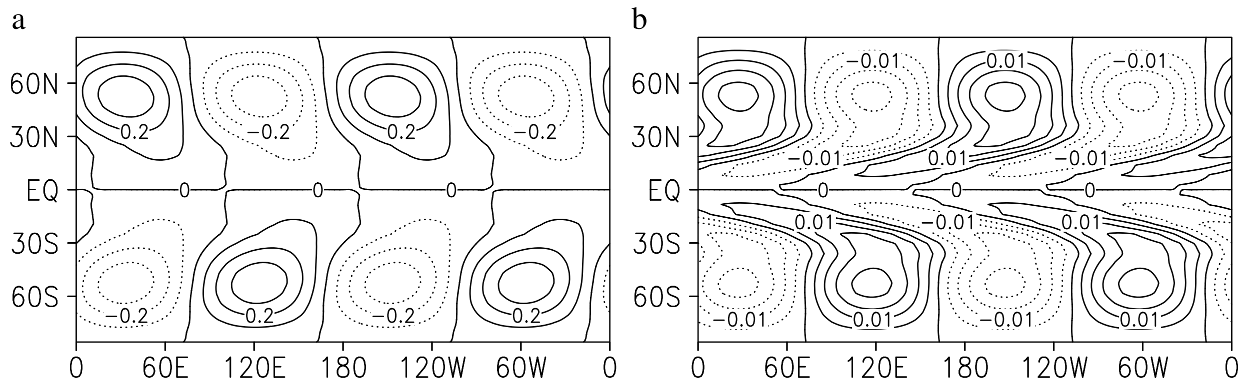

FIG. 3. Time mean zonally asymmetric potential temperature at 1 km (a) and at 9 km (b) height.

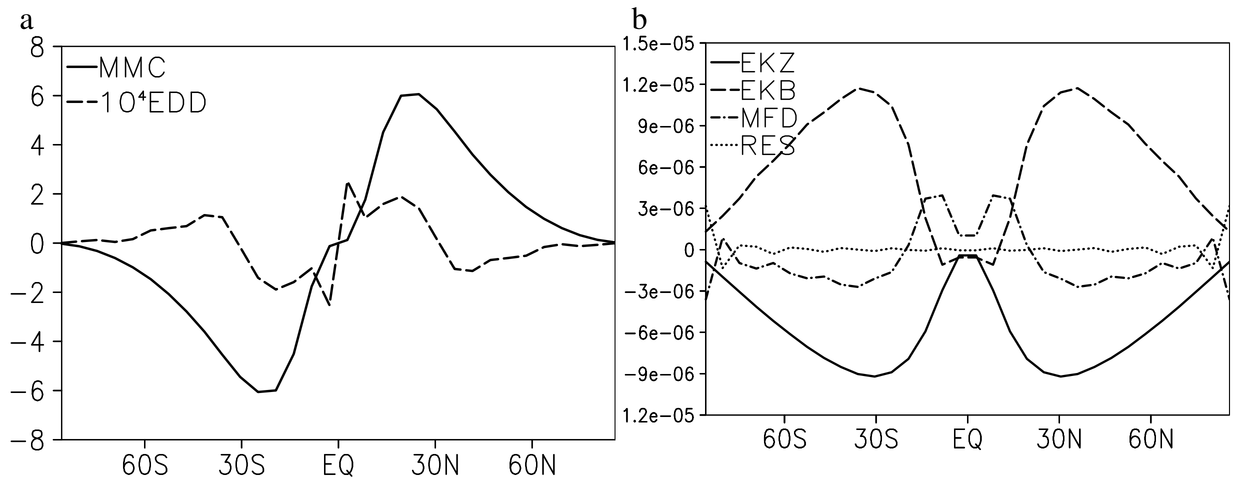

FIG. 4. (a) Zonally and vertically averaged time mean meridional momentum flux $\langle u'v' \rangle_{z,\lambda}$ by the mean meridional overturning circulation (MMC) and by the eddies ($10^4 EDD$), where the magnitude of the eddy flux was multiplied by the factor 10^4 to make it visible on the scale. (b) Contributions in the stationary barotropic momentum equation (49): Ekman friction by the baroclinic (EKZ) and barotropic (EKB) surface wind, contribution from momentum flux divergence and metric term (MFD) and residuum (RES). See text for details.

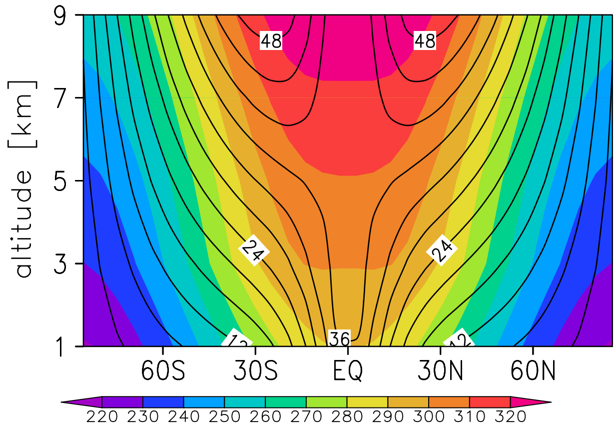

FIG. 5. Time mean zonal mean zonal wind (contours) and potential temperature (shading) in a simulation without the closure equation (39).

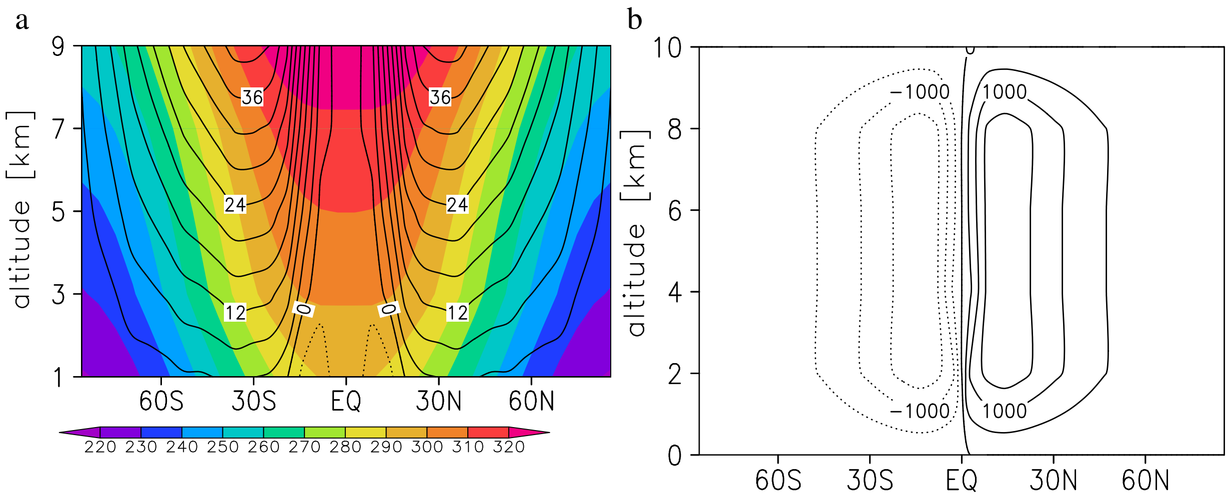

FIG. 6. Same as in Fig. 2 but for a simulation with diffusion coefficient K confined in the tropics, see eq. (50).

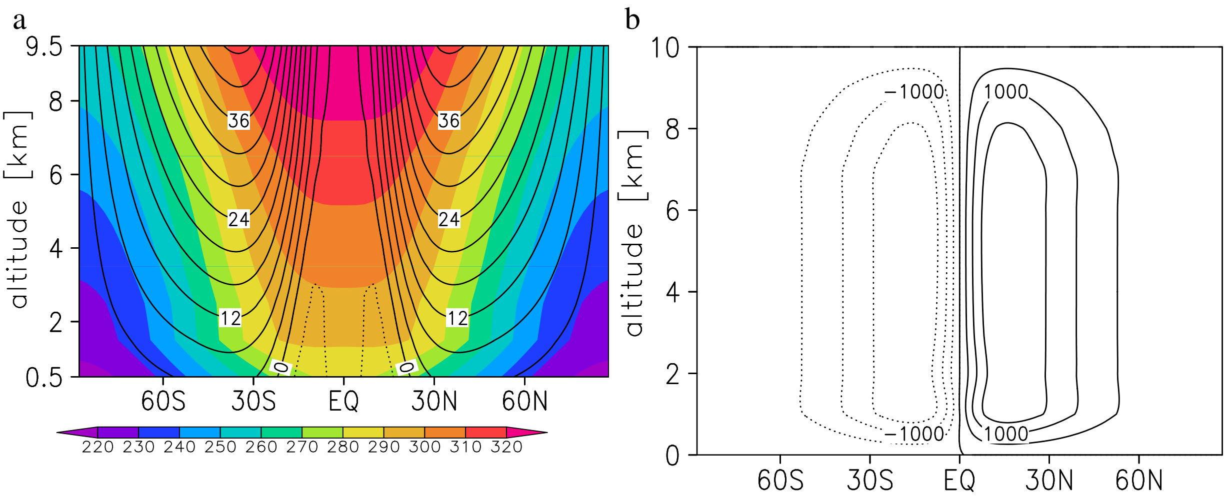

FIG. 7. Same as in Fig. 2 but for a simulation with T42 spectral resolution and ten vertical levels.

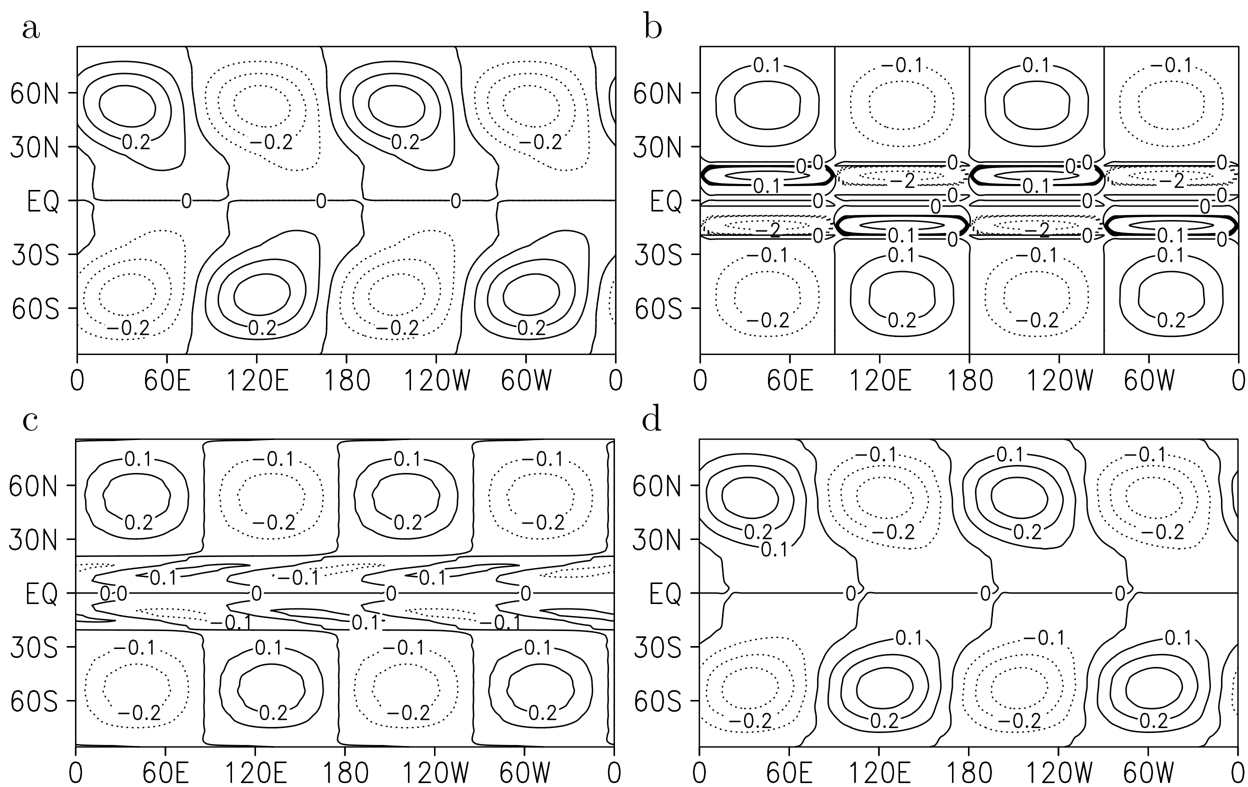

FIG. 8. Time mean zonally asymmetric potential temperature at 1 km height: (a) nonlinear simulation, (b) analytical solution (65), (c) inviscid linear model and (d) the linear model. See text for explanation of the different models. Note that in Fig.8 b also the ± 2 contour line is drawn to indicate the large amplitudes around $15°$.

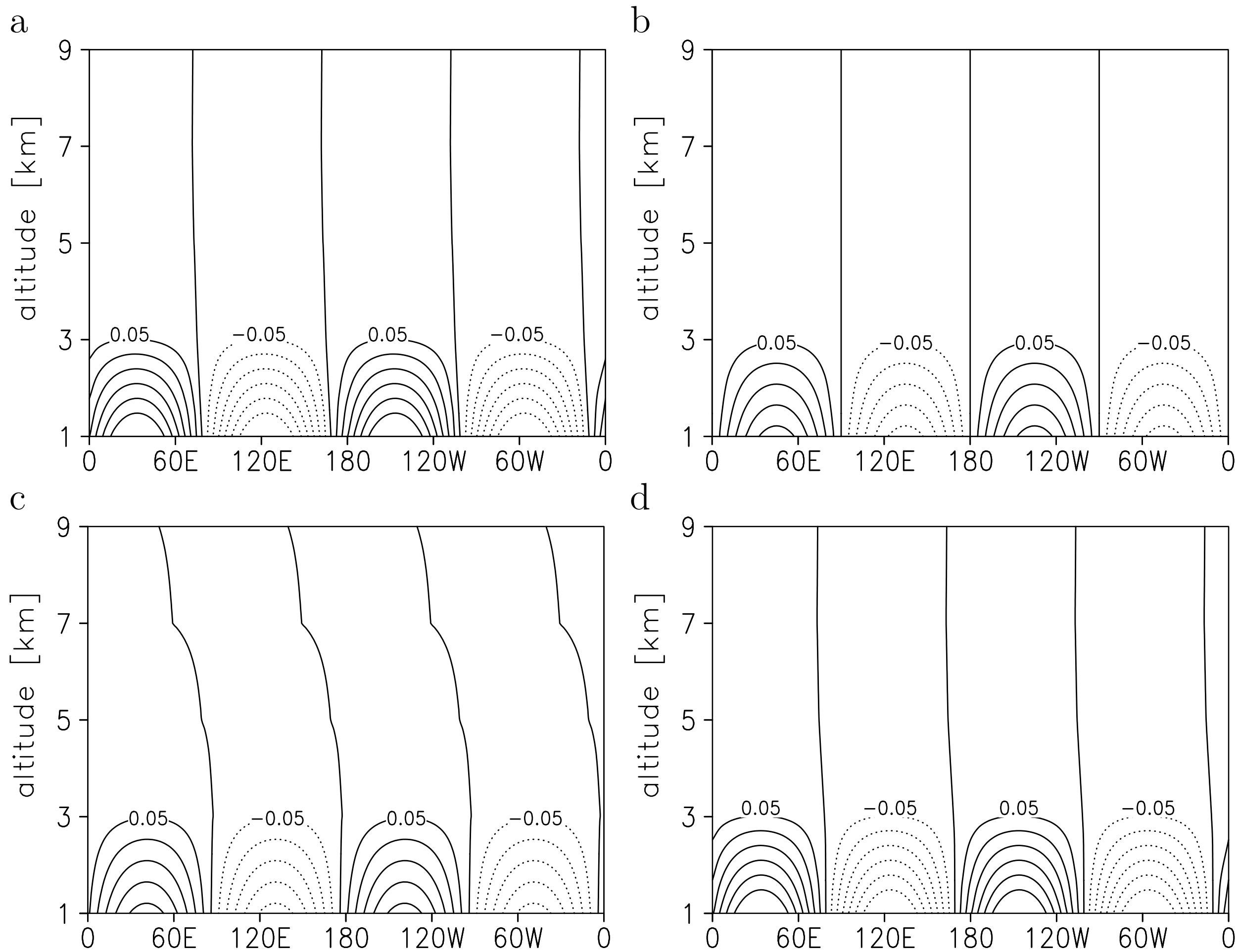

FIG. 9. Longitude-height cross-section at 50° N of time mean zonally asymmetric potential temperature: (a) nonlinear simulation, (b) analytical solution (65), (c) inviscid linear model and (d) the linear model.

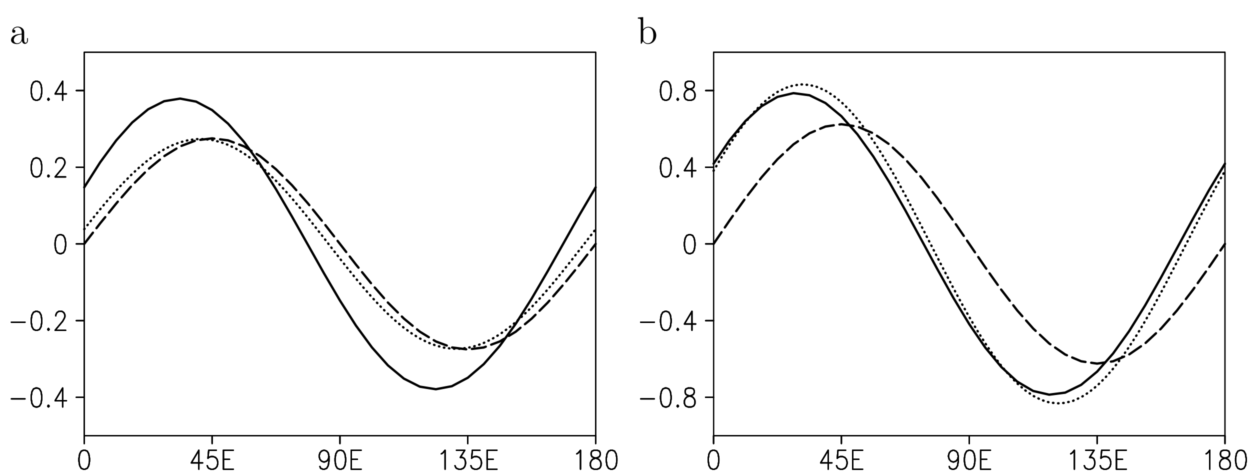

573 FIG. 10. Time mean zonally asymmetric potential temperature as a function of longitude at 50° N and 1 km
574 height from the nonlinear model (solid line), linear inviscid model (dotted line) and analytical solution (dashed
575 line): for a relaxation time scale of 15 days (a) and of 5 days (b).

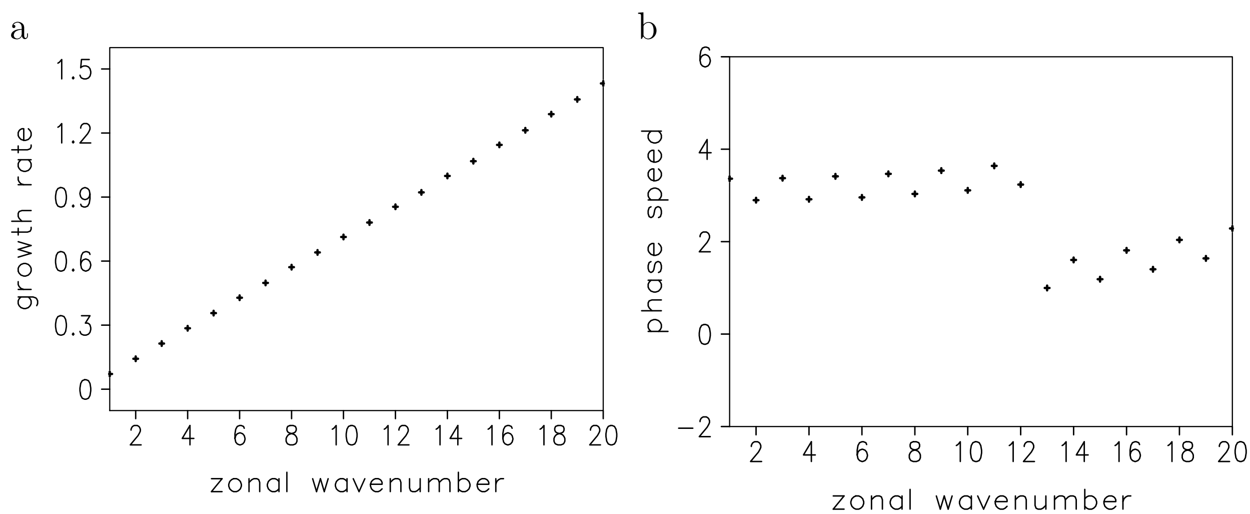

576 FIG. 11. (a) Growth rate [day^{-1}] and (b) phase speed [ms^{-1}] corresponding to the most unstable mode as a
577 function of zonal wavenumber.

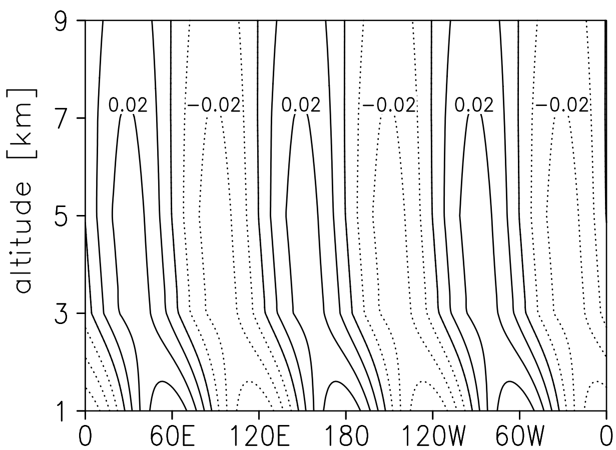

578 FIG. 12. Longitude-height cross-section at 50° N of the real part of most unstable mode with zonal wavenum-
579 ber 3, in units of θ_0.